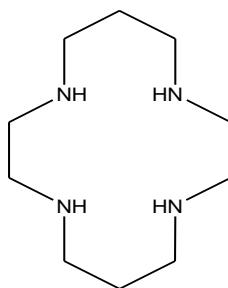


# CHAPTER 2

## THEORY AND LITERATURE REVIEW

### 2.1. Introduction

This research was focussed on the synthesis and characterization of copper(II) cyclam carboxylates (cyclam = 1,4,8,11-tetraazacyclotetradecane, **Figure 2.1**). The carboxylates were alkylcarboxylates ( $C_nH_{2n+1}COO$ ;  $n = 6, 7, 9, 11, 13, 15$ ) and  $CH_3(CH_2)_7CH((CH_2)_5CH_3)$ , and arylcarboxylates ( $p-XC_6H_4COO$  ( $X = NH_2, OH, OCH_3, CH_3, CN, H$ ) and  $C_6F_5$ ). These complexes were designed to be thermally stable, magnetic, and have liquid crystalline properties (for the former). The correlation between structure and physical properties (for alkylcarboxylates) or the electronic effect of a substituent (for arylcarboxylates) on the aromatic ring was investigated. Accordingly, the chapter covers the chemistry of copper(II) carboxylates, cyclam and its derivatives, and the concept of molecular modelling.



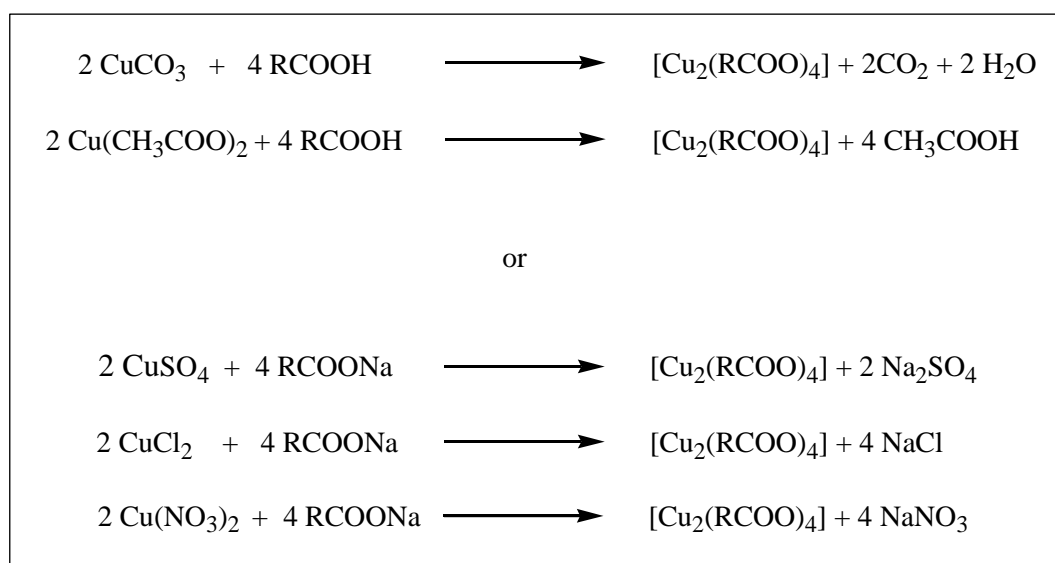
**Figure 2.1** The structural formula of cyclam

### 2.2. Copper(II) carboxylates

Copper is a transition metal bearing the electronic configuration of  $[Ar]4s^13d^{10}$ . Its common oxidation states are  $Cu^+$  ( $d^{10}$ ) and  $Cu^{2+}$  ( $d^9$ ), and in some rare cases,  $Cu^{3+}$  ( $d^8$ ) as well as  $Cu^{4+}$  ( $d^7$ ) ion [1]. However, the most stable oxidation state is that of  $Cu^{2+}$  ion, and hence its complexes have been studied comprehensively in many different research

fields, encompassing biomedicine [2,3] metalloenzyme and catalysis [4]. However, particular interest was on their magnetic properties [5-8]. This is mainly because  $\text{Cu}^{2+}$  ion carries only one unpaired electron, making the interpretation of the magnetic interaction of the associated complexes relatively easier compared to those with more unpaired electrons.

Vast numbers of copper(II) complexes are known. A large group involves carboxylate ligands, both aliphatic and aromatic, forming dimeric complexes of general formula  $[\text{Cu}_2(\text{RCOO})_4]$ . The facile syntheses of these carboxylates are well documented in the literature. They could be prepared either by reaction of basic copper(II) carbonate or copper(II) acetate with corresponding carboxylic acids [9-11], or by reaction of a copper(II) salt (sulphate, chloride, nitrate) with the sodium salt of the carboxylic acid [5,12] (**Scheme 2.1**).



**Scheme 2.1** Reaction equations for the formation of  $[\text{Cu}_2(\text{RCOO})_4]$  [5,12].

In most cases, the resultant binuclear complexes were shown to adopt a paddle-wheel structure (**Figure 2.2**), where each copper(II) centre is bridged by four bidentate carboxylate ligands through their oxygen atoms, and forming the basal plane of the complex.

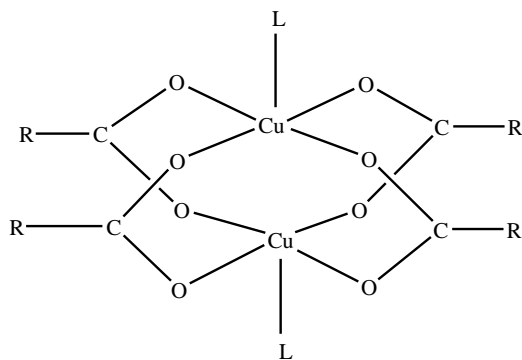


**Figure 2.2** Schematic view of the typical paddle-wheel structure of  $[\text{Cu}_2(\text{RCOO})_4(\text{L})_2]$ ; L is most often solvent molecules

In the paddle-wheel structure shown, the axial position is either occupied by solvent molecules such as methanol [9], ethanol, acetone, acetonitrile [13], pyridine [14], and dimethylformamide [15], by adducts, such as nicotinamide [10], benzothiazole [12], 2,2'-bipyridine and phenanthroline [15], or by oxygen atom of another dimeric unit, forming an oligomeric chain (**Figure 2.3**) [16].

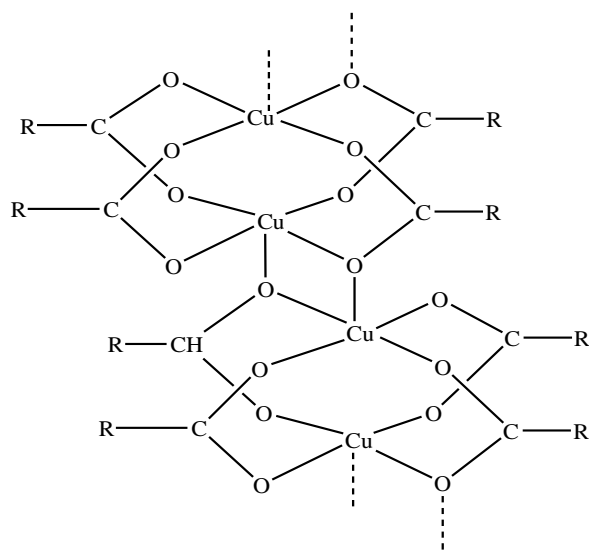


**Figure 2.3** An oligomeric structure of  $[\text{Cu}_2(\text{RCOO})_4]$ , showing only two dimers [16].

The study of crystal structure of copper(II) carboxylate containing saturated alkane started back in 1972 by Bird and Lomer, where they have successfully deduced the structure of anhydrous copper(II) butanoate,  $[\text{Cu}_2(\text{CH}_3(\text{CH}_2)_2\text{COO})_4]$  [17]. They

however quoted that copper(II) carboxylate complexes with higher number of alkyl chain would unfavourably form single crystals. Nevertheless in 1974, Lomer together with Perera have successfully obtained crystals of anhydrous copper(II) decanoate ( $[\text{Cu}_2(\text{CH}_3(\text{CH}_2)_8\text{COO})_4]$ ) and copper(II) octanoate ( $[\text{Cu}_2(\text{CH}_3(\text{CH}_2)_6\text{COO})_4]$ ) by using a gel diffusion method. All three complexes crystallized in triclinic polymorph of *P*-1 space group [18,19].

In 2008, Ramos *et al.* again reported the crystal structure of anhydrous copper(II) decanoate (**Figure 2.4**). Using an advanced crystal software package, they have been able to provide a better molecular representation of the structure. The complex crystallized in two different polymorphs depending on the crystallizing solvent. Crystals with triclinic polymorphs were obtained from *n*-heptane, while monotropic polymorphs were obtained from ethanol. Both crystalline polymorphs still however mutually belong to the identical space group of *P*-1 [20].

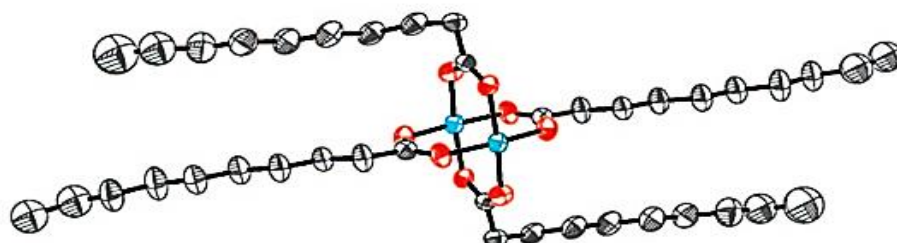


**Figure 2.4** Crystal structure of copper(II) decanoate,  $[\text{Cu}_2(\text{CH}_3(\text{CH}_2)_8\text{COO})_4]$ ; hydrogen atoms were not shown [20].

Prior to that, there was an investigation on the interaction of copper(II) heptanoate, octanoate, nonanoate, decanoate and dodecanoate with pyridine adducts, followed by an addition of water to the respective copper(II) alkanoate-pyridine complexes [21]. The findings showed that only copper(II) nonanoate-pyridine formed stable crystals upon addition of water. The formerly dimeric  $[\text{Cu}_2(\text{CH}_3(\text{CH}_2)_7\text{COO})_4(\text{py})_2]$  had structurally rearranged into a mononuclear complex,

[Cu(CH<sub>3</sub>(CH<sub>2</sub>)<sub>7</sub>COO)<sub>2</sub>(py)<sub>2</sub>(H<sub>2</sub>O)] with square pyramidal environment around the copper centre (**Figure 2.5**).

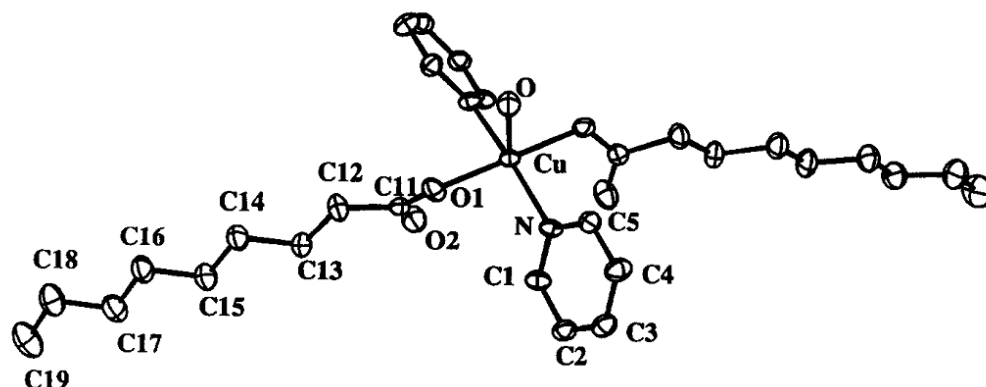


**Figure 2.5** ORTEP view of the structure [Cu(CH<sub>3</sub>(CH<sub>2</sub>)<sub>7</sub>COO)<sub>2</sub>(py)<sub>2</sub>(H<sub>2</sub>O)] with atom labelling scheme, hydrogen atoms were not drawn [21].

However when similar reaction of the respective copper(II) alkanoate with ammonia adducts [22] was carried out, the mononuclear complex obtained, [Cu(CH<sub>3</sub>(CH<sub>2</sub>)<sub>8</sub>COO)<sub>2</sub>(NH<sub>3</sub>)<sub>2</sub>].H<sub>2</sub>O, showed an octahedral geometry with extreme tetragonal distortion (**Figure 2.6**).

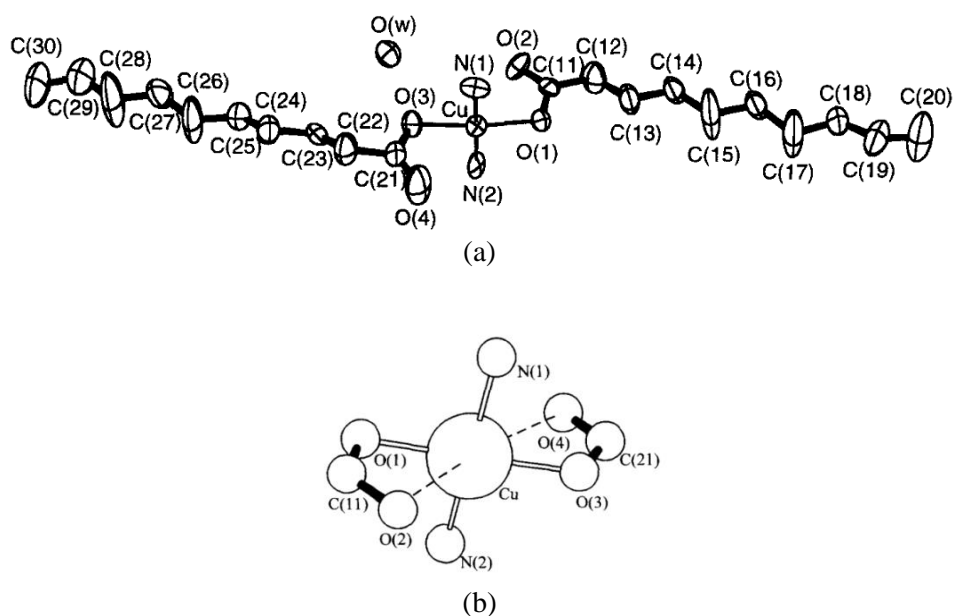


**Figure 2.6** (a) ORTEP view of [Cu(CH<sub>3</sub>(CH<sub>2</sub>)<sub>8</sub>COO)<sub>2</sub>(NH<sub>3</sub>)<sub>2</sub>].H<sub>2</sub>O with atom labelling scheme, hydrogen atoms were omitted; and (b) schematic presentation of the coordination environment around the copper atom [22].

Some examples of the structure of their aromatic analogues include diacetonitrile copper(II) *o*-nitrobenzoate,  $[\text{Cu}_2(\textit{o}\text{-NO}_2\text{C}_6\text{H}_4\text{COO})_4(\text{CH}_3\text{CN})_2]$  [10] (**Figure 2.7**) and dimethanol copper(II) *o*-fluorobenzoate,  $[\text{Cu}_2(\textit{o}\text{-FC}_6\text{H}_4\text{COO})_4(\text{CH}_3\text{OH})_2]$  [16] (**Figure 2.8**).

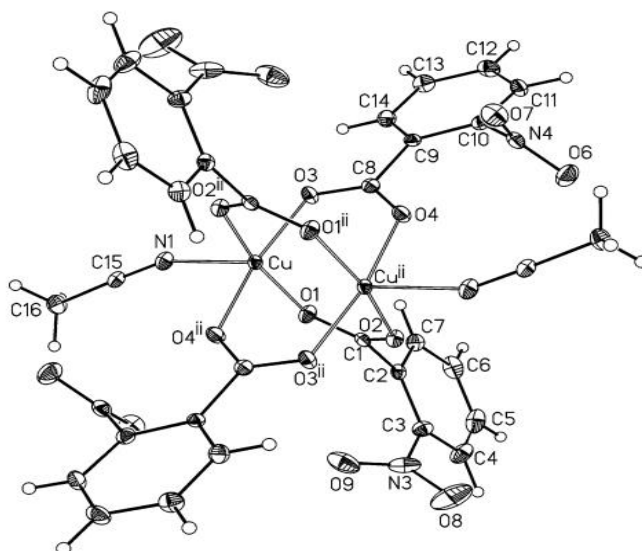


**Figure 2.7** Crystal structure of  $[\text{Cu}_2(\textit{o}\text{-NO}_2\text{C}_6\text{H}_4\text{COO})_4(\text{CH}_3\text{CN})_2]$  [10].

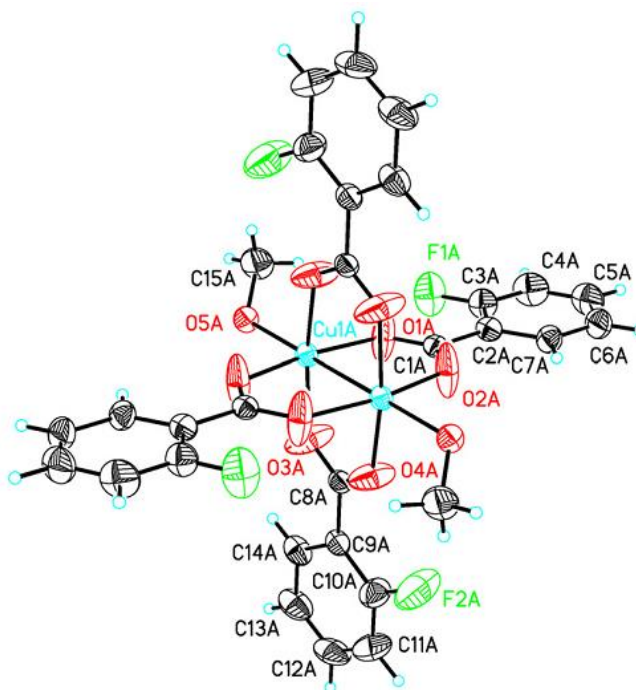


**Figure 2.8** Crystal structure of  $[\text{Cu}_2(\textit{o}\text{-FC}_6\text{H}_4\text{COO})_4(\text{CH}_3\text{OH})_2]$  [16].

An example of oligomeric copper(II) carboxylate is copper(II) trifluoropentanoate,  $[\text{Cu}_2(\text{CF}_3(\text{CH}_2)_3\text{COO})_4]$  (**Figure 2.9**) [16].

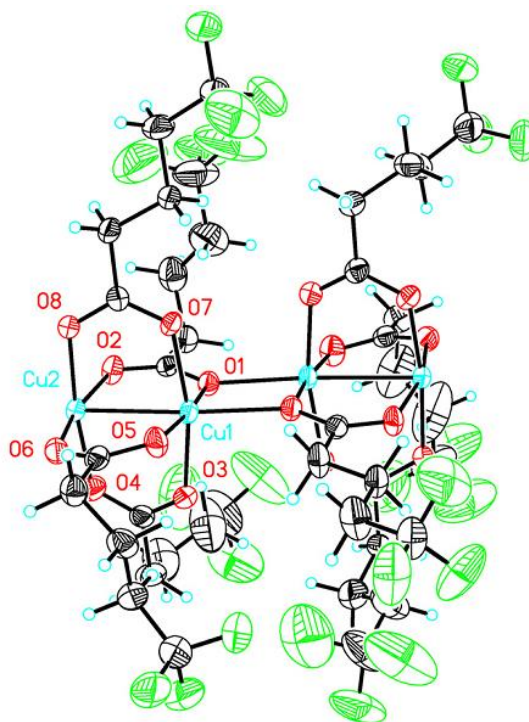


**Figure 2.9** Crystal structure of  $[\text{Cu}_2(\text{CF}_3(\text{CH}_2)_3\text{COO})_4]$ , showing two paddlewheel structures [16].

### 2.3. Cyclam

Cyclam (1,4,8,11-tetraazacyclotetradecane) is a 14-membered ring polyazamacrocyclic (Figure 2.10). It is a tetradentate aza-N donors which form an equatorial basal plane with five- and six-membered chelate rings arranged alternately. In the coordination with metal complexes, cyclam shows strong affinity towards transition metals rather than alkali and alkaline earth metals [23].

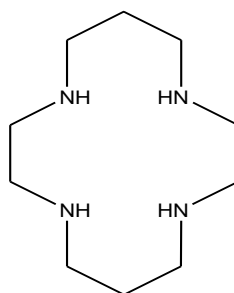


**Figure 2.10** The schematic representation of cyclam

As relatively opposed to its open-chain analogues, cyclam is an easily functionalized ligand and would exhibit enhanced structural stabilities with metal complexes, since the metal ion is firmly held within its cavity. Therefore, the coordination complexes formed would not be easily impaired by metal dissociation [23] (**Appendix 4**).

Bosnich's nomenclature had conceptually described the stereochemistry of cyclam coordination complexes in octahedral geometry with respect to the N–H bond direction relative to the basal plane. Since each coordinated nitrogen atom is chiral, five distinct *cis* and *trans* isomers are possible. The five isomers are commonly denoted as I–V, or alternatively by the chirality of the four aza-N atoms based on the (*R,S*)-nomenclature (**Figure 2.11**) [24].

The *trans*-III isomer is deduced as the most stable among the five possible configurations, in which cyclam is folded in its lowest energy, where the six-membered chelate ring adopts the least-strained chair conformation and the five-membered chelate ring is staggered in gauche conformation. The calculated relative energies of the five configurations are given in **Table 2.1** [25]. The average C–N bond length is 1.461(6) Å [26].

**Table 2.1** Relative energies calculated for the five isomers of cyclam [25].

Configuration	Energy (kJ mol <sup>-1</sup> )
I ( <i>R,S,R,S</i> )	2.13
II ( <i>R,S,R,R</i> )	1.00
III ( <i>R,R,S,S</i> )	0.00
IV ( <i>R,S,S,R</i> )	1.96
V ( <i>R,R,R,R</i> )	2.13



In essence, the flexibility of cyclam to host a wide range of guest metal ions with large association constant has developed spectacular growth to the synthesis of various coordinated transition metal complexes, particularly of comprising carboxylates as the counter ions. The resulting complexes are naturally mononuclear, as the cavity site radius of cyclam could perfectly accommodate one metal ion [23].

In the nature of interactions of carboxylate groups with the core metal centre, the  $O_{\text{carboxyl}}$  atoms might either show coordination tendency towards the metal, or might not be directly coordinated, hence exist as free ions. For instance, complexation of zinc(II) cyclam with maleate (two carboxylate groups are mutually *cis* across the C=C bond) and fumarate (two carboxylate group are *trans* to each other) have shown distinctive coordination behaviours [27].

In  $[\text{Zn}(\text{cyclam})(\text{cis-OOCCH}=\text{CHCOO})]$ , the zinc(II) ion and maleate ligand are directly coordinated. The presence of hydrogen bonding between the N–H groups of the macrocycle and uncoordinated oxygen atom of the ligand connects two macrocycles, resulting in the formation of a one-dimensional coordination polymer (**Figure 2.12**). Both complexes were synthesized by adding aqueous solution of sodium maleate and sodium fumarate to solution of  $\text{Zn}(\text{cyclam})(\text{ClO}_4)$  in DMF, respectively

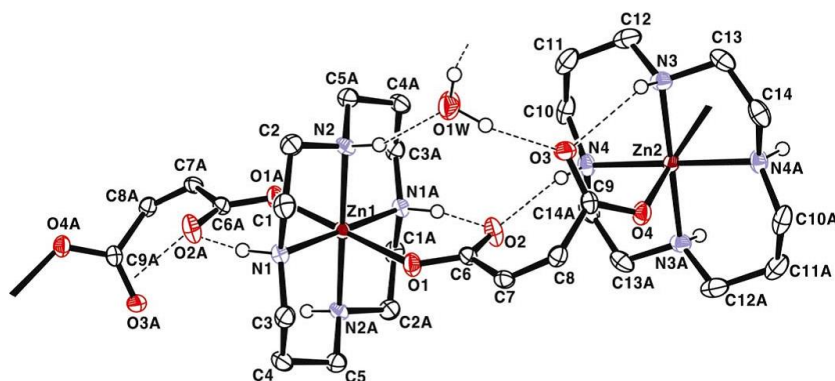


**Figure 2.12** Molecular structure of  $[\text{Zn}(\text{cyclam})(\text{cis-OOCCH}=\text{CHCOO})]$  with atom-labelling scheme; carboxylate groups are directly coordinated to zinc(II) ion [27].

As the basicity of fumarate is similar to that of maleate, it is unexpected to observe that it does not interact with zinc(II) cyclam. Instead, the axial positions of the cationic moiety are occupied by water molecules (**Figure 2.13**). Additionally,  $[\text{Zn}(\text{cyclam})(\text{H}_2\text{O})_2](\text{trans}\text{-OOCCH}=\text{CHCOO})$  unfavourably formed an additional hydrogen bond interactions as observed in its isomeric counterpart.

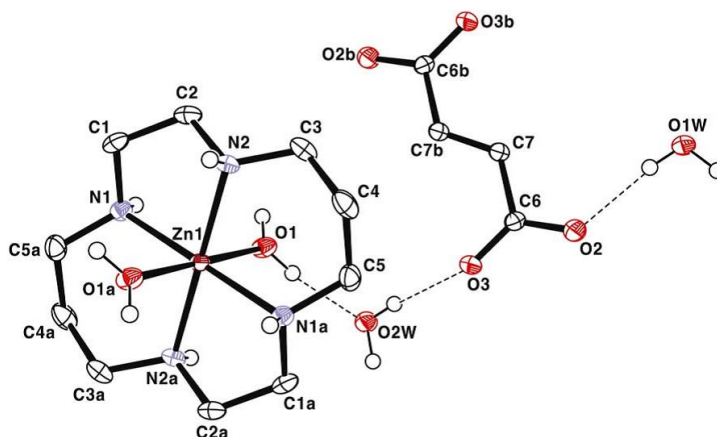


**Figure 2.13** Molecular view of  $[\text{Zn}(\text{cyclam})(\text{H}_2\text{O})_2](\text{trans}\text{-OOCCH}=\text{CHCOO})$  with atom-labelling scheme; fumarate anion is not coordinated to Zn atom [27].

Similar molecular interaction was observed when the fumarate anion was reacted with nickel(II) cyclam. An example is  $[\text{Ni}(\text{cyclam})(\text{H}_2\text{O})_2](\text{trans}\text{-OOCCH}=\text{CHCOO})\cdot 4\text{H}_2\text{O}$  (**Figure 2.14**). The complex was prepared by a one-pot reaction of nickel(II) chloride hexahydrate, cyclam and sodium fumarate dissolved in water and heated overnight in a water bath [28].

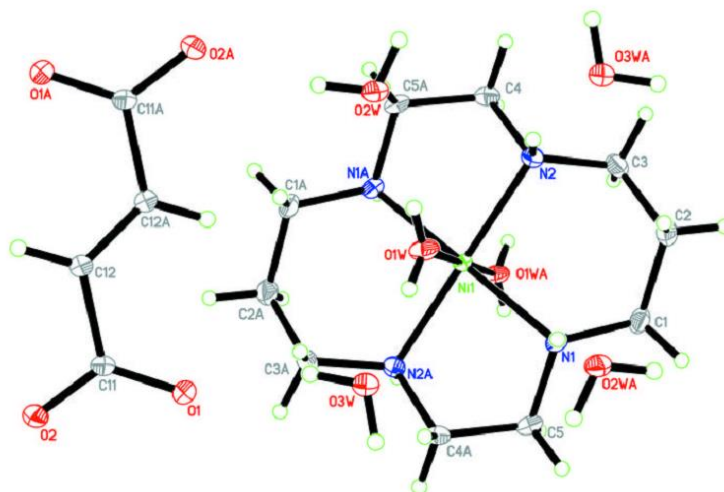


**Figure 2.14** Molecular structure of  $[\text{Ni}(\text{cyclam})(\text{H}_2\text{O})_2](\text{trans-OOCHC}=\text{CHCOO})\cdot 4\text{H}_2\text{O}$ ; Ni(II) ion in the cyclam is six-coordinated with distorted octahedral geometry with four *aza*-N atoms in the equatorial plane and water molecules in the apices [28].

However, in the complexation of Ni(II) cyclam with benzoate ligand, the carboxylate groups were found to bind directly to the Ni atom, orientated axially above and below the macrocycle plane (**Figure 2.15**). The complex  $[\text{Ni}(\text{cyclam})(\text{C}_6\text{H}_5\text{COO})_2]$  was prepared by adding solid nickel carbonate tetrahydrate to a hot methanolic solution of benzoic acid [29].

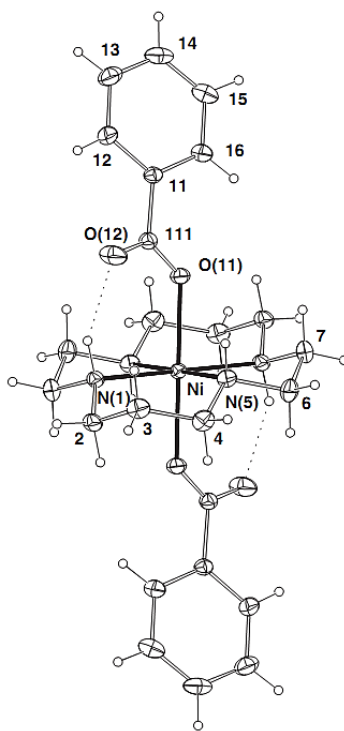


**Figure 2.15** Molecular structure of  $[\text{Ni}(\text{cyclam})(\text{C}_6\text{H}_5\text{COO})_2]$ , showing direct coordination between Ni atom and carboxylate groups [29].

The structures of cyclam complexes are also extended to copper(II) carboxylates. Some reported structures include copper(II) cyclam benzoate,  $[\text{Cu}(\text{cyclam})(\text{H}_2\text{O})_2](\text{C}_6\text{H}_5\text{COO})_2 \cdot 2\text{H}_2\text{O}$  (**Figure 2.16**) [29] and pentafluorobenzoate  $[\text{Cu}(\text{cyclam})(\text{H}_2\text{O})_2](\text{C}_6\text{F}_5\text{COO})_2 \cdot 2\text{H}_2\text{O}$  (**Figure 2.17**) [30]. In both complexes, water molecules are the competitive electron donor against the carboxylates.

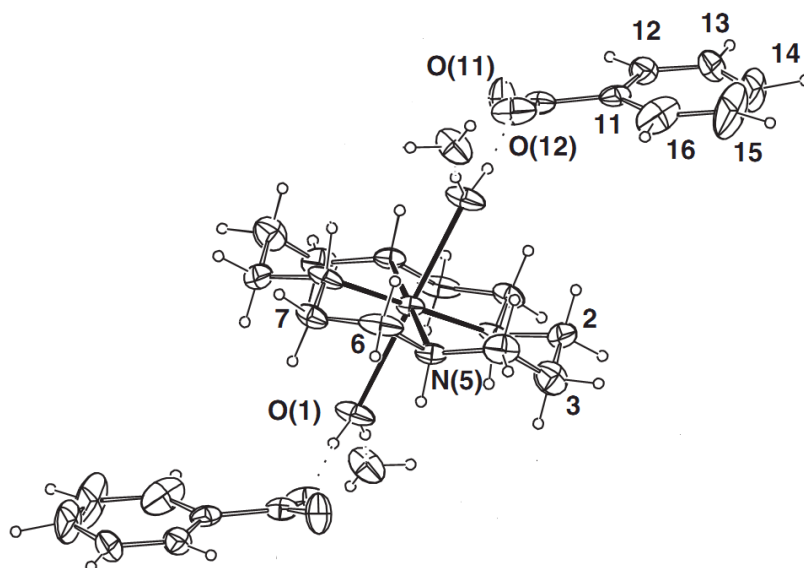


**Figure 2.16** Molecular structure of  $[\text{Cu}(\text{cyclam})(\text{H}_2\text{O})_2](\text{C}_6\text{H}_5\text{COO})_2 \cdot 2\text{H}_2\text{O}$  [29].

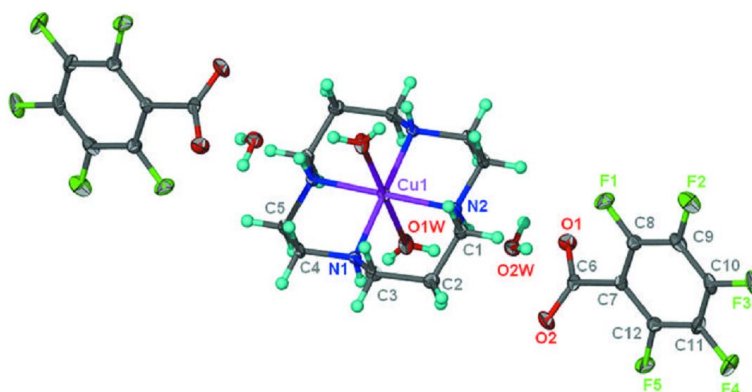
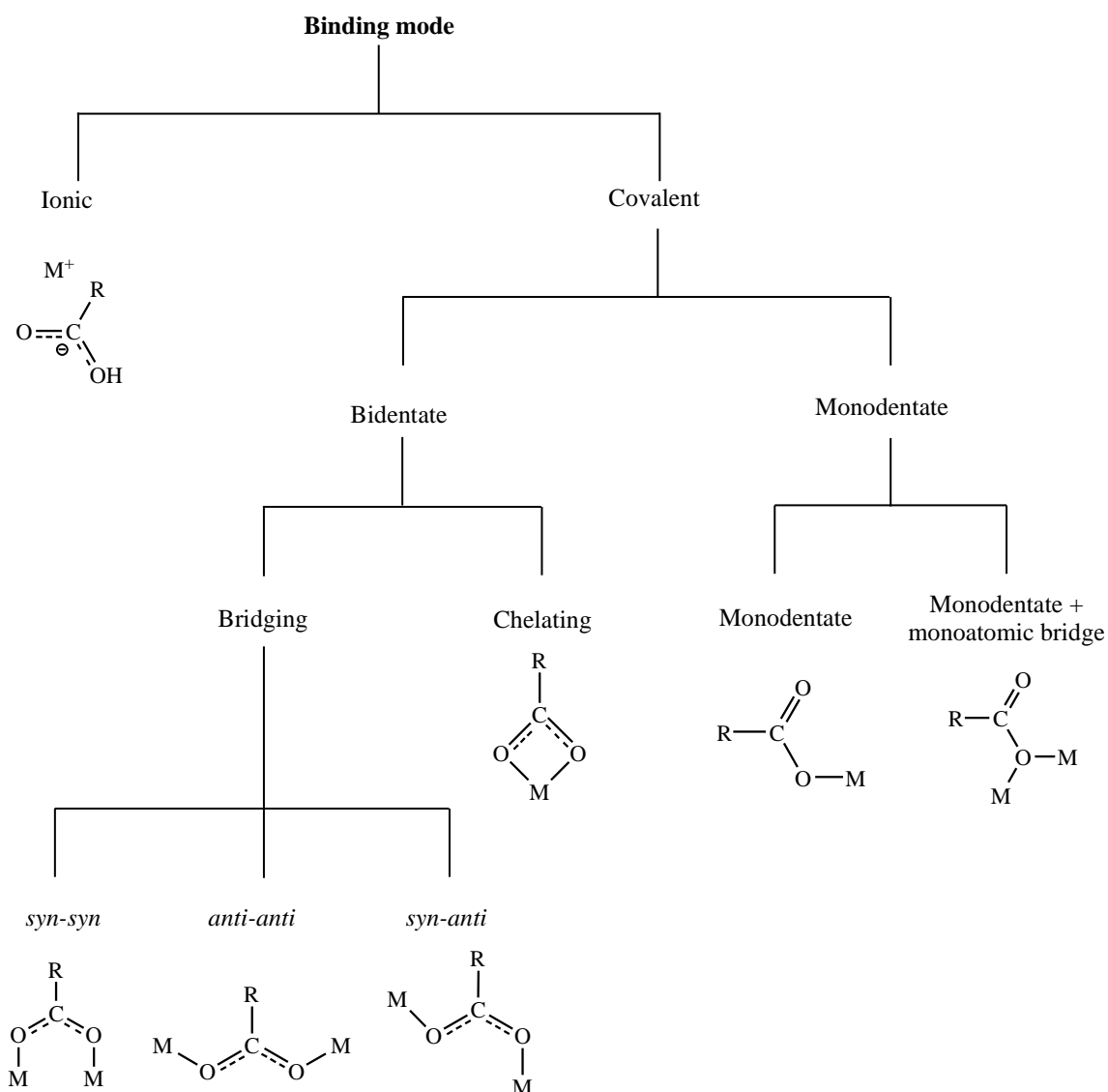


**Figure 2.17** Molecular structure of  $[\text{Cu}(\text{cyclam})(\text{H}_2\text{O})_2](\text{C}_6\text{F}_5\text{COO})_2 \cdot 2\text{H}_2\text{O}$  [30].

#### 2.4. Fourier Transform Infrared Spectroscopy

The carboxylate ion,  $\text{RCOO}^-$ , can accommodate a versatile binding mode in its coordination towards the metal centre. This can be considered to span into ionic, monodentate, bridging chelating as well as bridging bidentate with *syn-syn*, *anti-anti* or *syn-anti* configuration [31] (**Scheme 2.2**).



**Scheme 2.2** Different binding mode of carboxylate ion [31].

The assignment of the mode of carboxylate binding is often based on IR spectroscopy [32-34]. A typical infrared spectrum showing the position of asymmetric and symmetric carboxylate stretching band ( $\bar{\nu}_{as,COO}$  and  $\bar{\nu}_{s,COO}$  respectively) are depicted in **Figure 2.18**

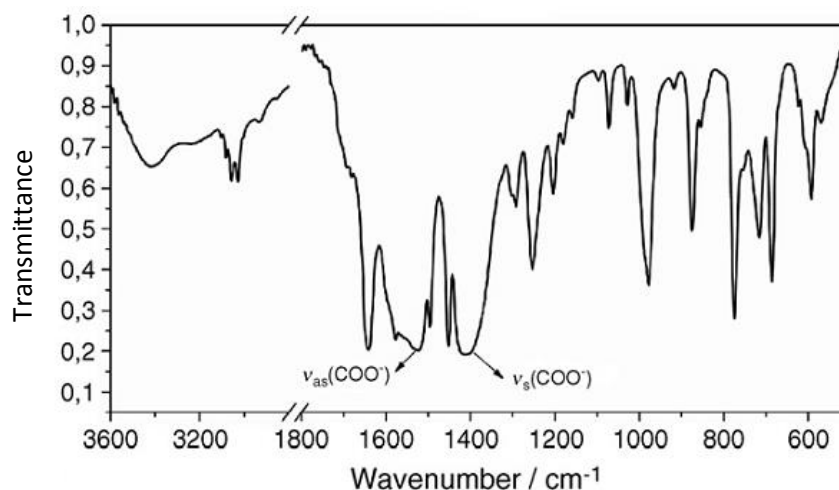


**Figure 2.18** An infrared spectrum showing the position of COO stretching band [31].

As such, for a given complex, the type of binding mode is identified by calculating the magnitude of separation between the asymmetric and symmetric stretches of the carboxylate group,  $\Delta_{\text{COO}} = \bar{\nu}_{\text{as,COO}} - \bar{\nu}_{\text{s,COO}}$ . The frequency value of  $\bar{\nu}_{\text{as,COO}}$  is found in the range of  $\sim 1541\text{-}1678\text{ cm}^{-1}$ , whereas that of  $\bar{\nu}_{\text{s,COO}}$  is within  $\sim 1202\text{-}1417\text{ cm}^{-1}$  [35]. In general, the trend of the separation value is suggested as:

$$\Delta(\text{chelating}) < \Delta(\text{bridging}) < \Delta(\text{ionic}) < \Delta(\text{monodentate})$$

where the  $\Delta(\text{ionic})$  value is approximately  $170\text{ cm}^{-1}$  (for acetates) [36,37]. The  $\Delta_{\text{COO}}$  value of less than  $120\text{ cm}^{-1}$  is frequently observed for chelating carboxylate group, while the  $\Delta_{\text{COO}}$  value of higher than  $180\text{ cm}^{-1}$  is commonly related to monodentate carboxylates. For compounds with bridging carboxylate, the value of  $\Delta_{\text{COO}}$  is observed within  $120\text{-}180\text{ cm}^{-1}$ . A comprehensive study of correlation of infrared spectra with different type of  $\text{RCOO}^-$  binding mode was reported by Zelenák *et al.* in 2006 [31], and is summarised in **Table 2.2**.

**Table 2.2** Wavenumbers of COO<sup>-</sup> stretches of Zn(II) complexes with different binding mode [31]

Binding mode	$\bar{\nu}_{\text{as,COO}}$	$\bar{\nu}_{\text{s,COO}}$	$\Delta_{\text{COO}}$
Chelating	1523	1411	112
Bridging ( <i>syn-syn</i> )	1572	1404	168
Bridging ( <i>syn-anti</i> )	1561	1376	185
Ionic	1570	1391	179
Monodentate	1630	1343	287

## 2.5. Electronic spectroscopy

Transition metals, notably those of the first-row metal ions, mostly form coloured complexes due to the electronic transitions between the *d* orbitals of the metals. It occurs when photon of light from visible range ( $\lambda = 400\text{-}780$  nm) of the electromagnetic spectrum, and its adjacent region, ultraviolet ( $\lambda = 200\text{-}400$  nm) and near infrared ( $\lambda = 780\text{-}1000$  nm), is introduced, providing an amount of energy that is sufficient to promote electrons from its ground state to a higher energy orbitals.

The amount of this absorbed energy at a certain wavelength produces absorption bands which could be studied directly by UV-visible spectroscopy. The bands are assigned to *d*→*d* transitions, ligand-to-metal charge transfer (LMCT) or metal-to-ligand charge transfer (MLCT).

In general, a *d*→*d* band is normally broad, and with weak intensities because it is naturally Laporte forbidden. Laporte's rule governs the selection of spectroscopic transitions of a molecule that contains an inversion centre, or so called centrosymmetric, such as octahedral and square planar complexes. It states that the electronic transition within the same orbital is forbidden as the parity is conserved.

However, the forbidden transitions are weakly allowed when the centre of inversion is disrupted, where the symmetry of the complexes will be distorted. This is commonly due to Jahn-Teller effect as well as vibronic transition. Therefore, the molar extinction coefficient,  $\epsilon$ , of these molecules is normally less than  $10 \text{ M}^{-1} \text{ cm}^{-1}$ . As a non-centrosymmetric molecule is not governed by this rule, tetrahedral or square pyramidal complexes will be more intensely coloured and their  $d \rightarrow d$  transition bands are relatively stronger with  $\epsilon \sim 100 \text{ M}^{-1} \text{ cm}^{-1}$ .

The value of  $\lambda_{\text{max}}$  (wavelength at maximum absorbance) of a  $d \rightarrow d$  absorption band is very useful in determining the geometry of a complex [38,39]. In particular, for copper(II) carboxylates, where the coordination environment at the metal centre is generally a square pyramidal, it is expected that the  $\lambda_{\text{max}}$  of complexes would be found at around  $\sim 700 \text{ nm}$  [40,41]. Shoulders at higher wavelengths appearing in ultraviolet region with  $\lambda_{\text{max}}$  around  $300 \text{ nm}$  is a typical characteristic of a binuclear copper(II) carboxylates [12]. To illustrate, **Figure 2.19** depicts the UV-vis spectrum of copper(II) acetate, showing an LMCT peak, a shoulder and a  $d \rightarrow d$  absorption band.

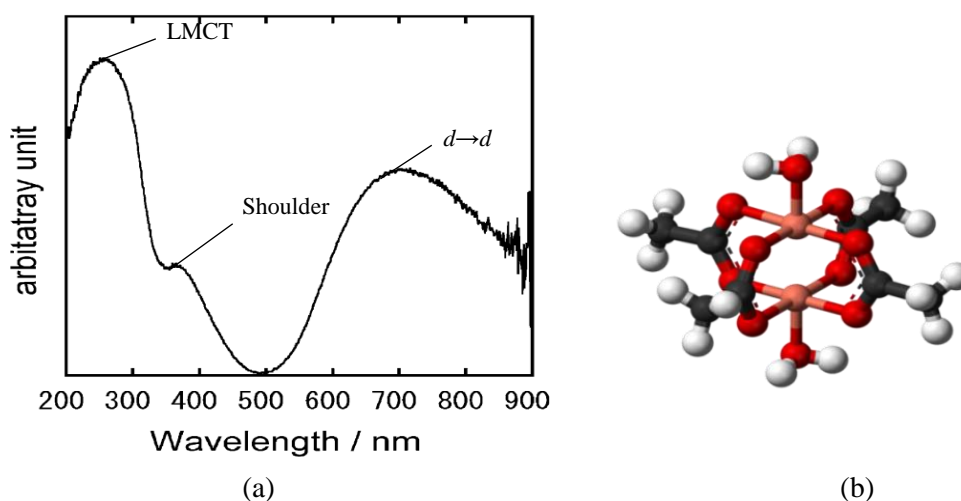


**Figure 2.19** (a) The UV-vis spectrum of copper(II) acetate,  $[\text{Cu}_2(\text{CH}_3\text{COO})_4(\text{H}_2\text{O})_2]$ ; and (b) the schematic view of the structure of the complex.

Pajtasova *et al.* in 2010 reported the correlation of aliphatic chain length of copper(II) carboxylates with their electronic spectra. The  $d \rightarrow d$  band of the studied complexes,  $[\text{Cu}_2(\text{CH}_3(\text{CH}_2)_n\text{COO})_4]$  ( $n = 10, 12, 14, 16$ ) ranges around 672–677 nm, and the band shifted to higher  $\lambda$  as the alkyl chain increases. This fact is related with the weakening of the Cu–O bond strength of the selected complexes [42]. The selected complexes also exhibit a shoulder, appearing in the ultraviolet region ( $\lambda_{\text{max}} \sim 362\text{--}373$  nm), which is an indicative of a binuclear complex. Intensive absorption at  $\lambda$  lower than 300 nm was also seen, an indication of charge transmission from carboxylic group to Cu(II) atoms (LMCT peak). However, the position of  $\lambda_{\text{max}}$  of these absorption bands was not influenced by the spacer chain length [12].

## 2.6. Magnetic properties

Electrons have a magnetic moment that can either be attracted or repulsed by a magnetic field, depending on whether the spin magnetic quantum number  $S$  is  $+1/2$  or  $-1/2$ . For an atom with a pair of electrons, each individual electron contributes to the overall spin magnetic quantum number and cancel each other, hence giving a zero net value of the total spin quantum number ( $S = 0$ ). Such species is said to be diamagnetic and will experience repulsion if placed between the poles of a strong magnetic field.

A paramagnetic material contains one or more unpaired electrons, thus the overall spin quantum number will be greater than zero ( $S > 0$ ). If a paramagnetic species is placed between the poles of the applied magnetic field, it will experience an attraction to the field.

Transition metals are denoted to have incompletely filled  $d$  orbitals with one or more unpaired electron(s), hence paramagnetic. The effective magnetic moment,  $\mu_{\text{eff}}$  results from both spin and orbital contribution of the unpaired electron(s). The expected

$\mu_{\text{eff}}$  for a particular metal ion can be estimated from the spin-only magnetic moment,  $\mu_{\text{eff}}$ , using the following relationship:

$$\mu_{\text{eff}} = \sqrt{n(n+2)} \quad (n = \text{number of unpaired electron})$$

For example, the value of  $\mu_{\text{eff}}$  for  $\text{Cu}^{2+}$  complexes is 1.73 BM. The unit is Bohr Magneton (BM). The  $\mu_{\text{eff}}$  value is calculated indirectly from the measured magnetic susceptibility,  $\chi$ , which represents the degree of magnetization of a material in response to an applied magnetic field. One of the most common techniques to calculate the value of  $\mu_{\text{eff}}$  is by using the Gouy method. The schematic representation of a Gouy magnetic balance is shown in **Figure 2.20**.

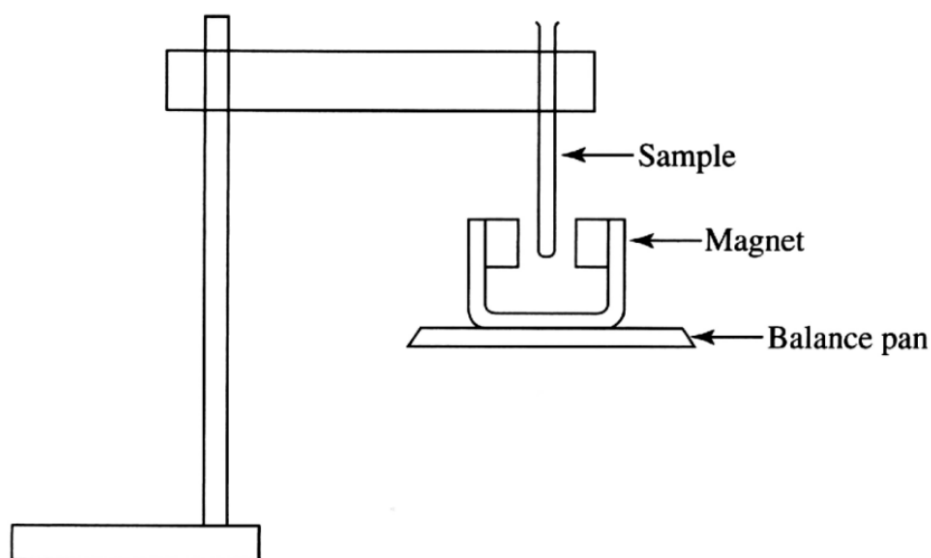


**Figure 2.20** Schematic representation of a Gouy balance

With an exception of hydrogen atom, all atoms or ions with unpaired electrons also have paired electrons. In an applied magnetic field, these paired electrons will induce diamagnetic moment and slightly mitigate the paramagnetic attraction. Therefore in every calculation, the overall effective moment should apply a subtractive diamagnetic correction,  $\chi_{\text{D}}$ . Values of  $\chi_{\text{D}}$  for some common atoms and ions is given in **Appendix 2**.

## 2.7. Thermal properties

Thermal analysis of copper(II) carboxylates are very important to deduce the stability of the complexes as a function of temperature and determine the phase transitions including evaporation, melting, decomposition, as well as glass transitions and mesomorphism. The thermal properties may be studied by thermogravimetric–differential thermal analysis (TG/DTA) together with differential scanning calorimetry (DSC), normally under nitrogen atmosphere.

For example, the thermogram of an aliphatic copper(II) carboxylate,  $[\text{Cu}_2(\text{CH}_3)(\text{CH}_2)_{16}\text{COO}]_4$  (**Figure 2.21**) shows that the complex was thermally stable when heated up to 220 °C. It shows a major degradation from 220 to 430 °C (~78%). However, DTA curve records an endothermic peak at 110 °C which is assigned to the phase transition of solid to liquid-crystal, an intermediate phase between solid and isotropic liquid. The final mass after its weight loss was 15%, and this corresponds to CuO residue. Likewise, the homologous complex with 16, 14 and 12 carbon chain length shows an endotherm peak at 114 °C, 117 °C and 108 °C respectively (**Table 2.3**) [43].

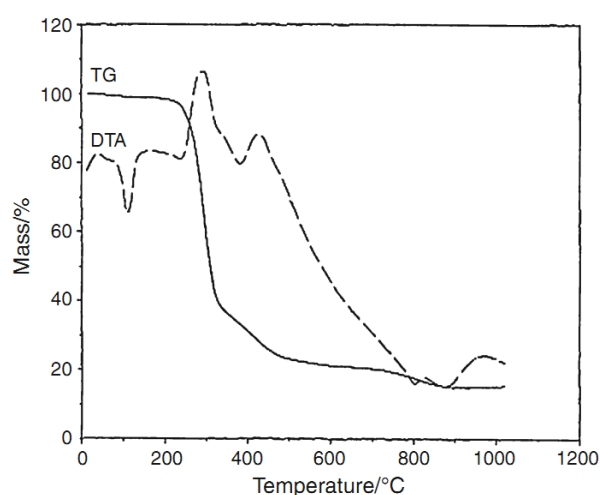


**Figure 2.21** TG/DTA curves of  $[\text{Cu}_2(\text{CH}_3)(\text{CH}_2)_{16}\text{COO}]_4$  [43].

**Table 2.3** Temperature of phase transitions from solid to liquid crystal mesophase from DTA and DSC, and enthalpy values of the selected copper(II) alkylcarboxylates [43].

Complex	DTA	DSC	
	T/°C	T/°C	$\Delta H/\text{kJ mol}^{-1}$
$[\text{Cu}_2(\text{CH}_3)(\text{CH}_2)_{10}\text{COO}]_4$	108	105	44.5
$[\text{Cu}_2(\text{CH}_3)(\text{CH}_2)_{12}\text{COO}]_4$	117	117	52.2
$[\text{Cu}_2(\text{CH}_3)(\text{CH}_2)_{14}\text{COO}]_4$	114	114	60.3
$[\text{Cu}_2(\text{CH}_3)(\text{CH}_2)_{16}\text{COO}]_4$	110	109	72.0

In addition, the thermal record of these complexes is complemented by DSC study. In the temperature range 50 – 200 °C, an endothermic peak of each of the selected complexes (**Figure 2.22**) were observed in a good agreement with DTA results (**Table 2.3**). The corresponding enthalpy changes ( $\Delta H$ ) throughout the heating process show a linear dependency with an increasing number of carbon chain [43].

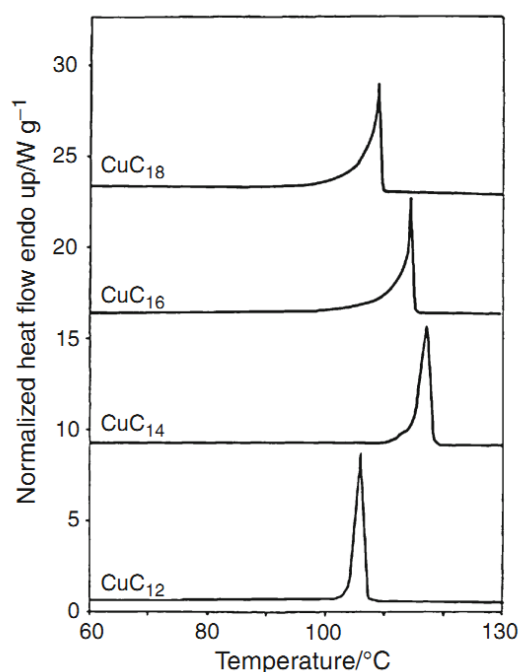


**Figure 2.22** DSC curves of  $[\text{Cu}_2(\text{CH}_3)(\text{CH}_2)_n\text{COO}]_4$  ( $n = 10, 12, 14$  and  $16$ ) [43]

This study has also focussed on thermotropic liquid crystals, in which phase transitions of a particular compound are observed as a function of temperature variation.

By convention, matter exists either as solid, liquid or gas. However, there is another significant state of matter that exists between the solid and liquid, and it exhibits properties that resemble both states. It has specific kind of order as in solid, but not as rigid so that it is still fluid like a liquid. This state of matter is called liquid crystal.

The discovery of liquid crystals is often referred to the work of Friedrich Reinitzer, who in 1888 reported that cholesteryl benzoate has two distinct melting points. In his experiment, he heated a solid sample and found that the compound did not directly melt in the same manner as other compounds. Instead, the solid was observed to change into hazy liquid, and as he further increased the temperature, the compound then became a clear, transparent liquid.

This feature was then attributed to describe the characteristic of typical liquid crystal materials. The hazy liquid state is defined as a mesophase. The temperature at which a material changes from solid into a mesophase is referred to as the melting point, while the temperature at which a mesophase turns into a transparent, isotropic liquid is referred to the clearing point. A material which displays such properties is said to exhibit mesomorphism.

Thermotropic liquid crystals can be divided into two types: calamitic (rod-like) or discotic (disk-like), depending on the framework of its building unit. The building unit of a liquid crystal material is called mesogen. Hence, if the liquid crystal materials contain metals, they are called metallomesogens.

Mesogen commonly consists of a rigid core with one or more flexible peripheral part [44]. The rigid moieties align the molecule in a particular angle and direction, and the flexible moieties, normally aliphatic chains, enhance fluidity. General examples of

calamitic and discotic mesogen are depicted in **Figure 2.23**, and their schematic representations are given in **Figure 2.24**.

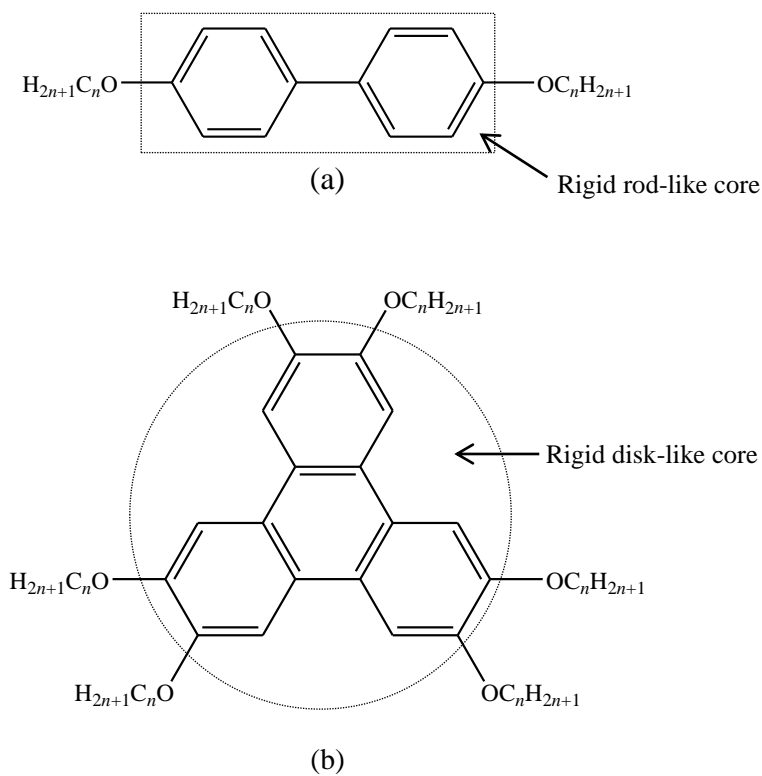


**Figure 2.23** Representative examples of: (a) calamitic; and (b) discotic mesogens

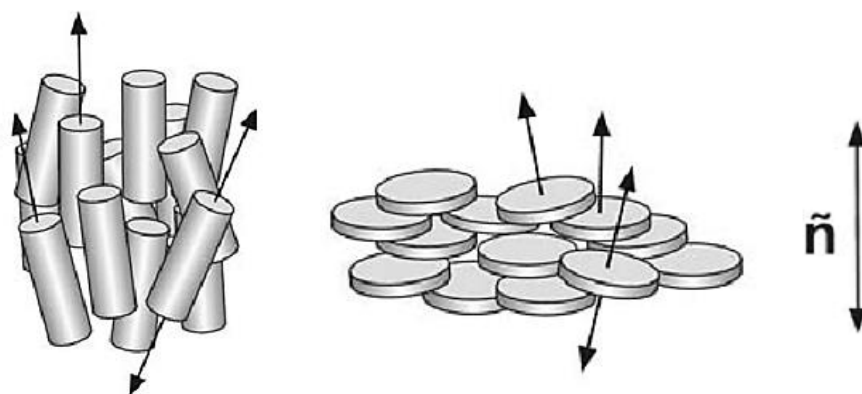


**Figure 2.24** Schematic representations of: (a) calamitic mesogen; and (b) discotic mesogen. Arrows indicate the axes of the molecules that align to the director  $n$ .

The mesophase of calamitic mesogen are divided into two classes: nematic and smectic phases. The nematic phase, abbreviated as  $N$ , is the least ordered and very fluid mesophase. Nematic phase could be observed under optical polarising microscope, usually displaying a schlieren texture [45] (**Figure 2.25**).

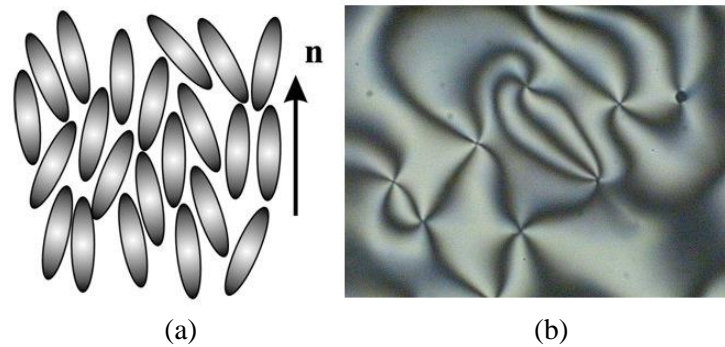


**Figure 2.25** (a) Schematic representation; and (b) schlieren texture of a nematic mesophase [45].

The smectic phases are more highly ordered and positionally oriented. There are a number of different types of smectic phases that have been recognised, but two most commonly found are smectic A ( $SmA$ ) and smectic C ( $SmC$ ). The schematic representation of the two phases is given in **Figure 2.26**.

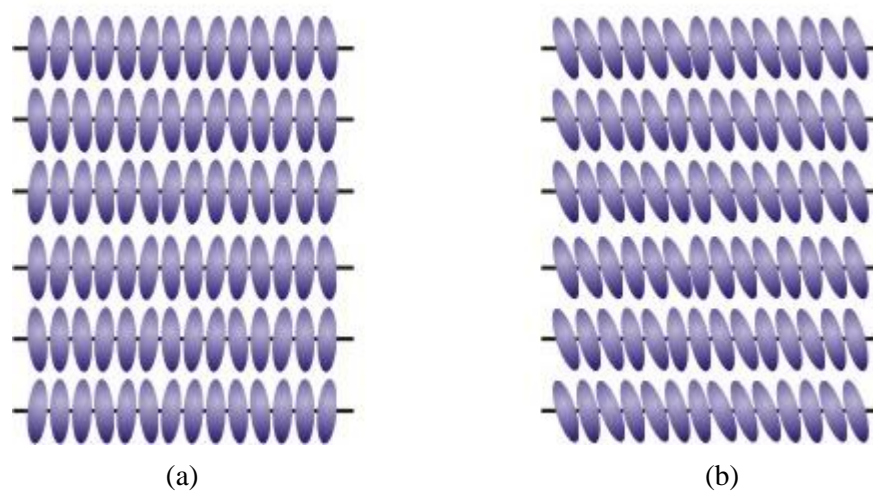


**Figure 2.26** Schematic representations of smectic phases, showing layered structure: (a)  $SmA$ ; and (b)  $SmC$  (tilted)

Since its initial discoveries, tremendous amounts of work have been done on calamitic liquid crystals. Examples are 2-alkoxy-5-phenylpyrimidines building unit with bromide terminal group and variation of spacer chain length [46] (**Figure 2.27**).

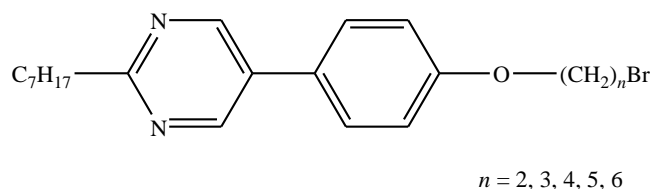


**Figure 2.27** 2-Alkoxy-5-phenylpyrimidines [46]

The mesomorphic properties for the above series of compounds were studied by a combination of differential scanning calorimetry and optical polarised microscopy. Upon cooling from an isotropic liquid, the compound with  $n = 5$  were observed to exhibit a fan-shaped texture, attributed as the SmA phase (**Figure 2.28**). The phase changes gave a typical DSC curve of a liquid crystalline material (**Figure 2.29**).

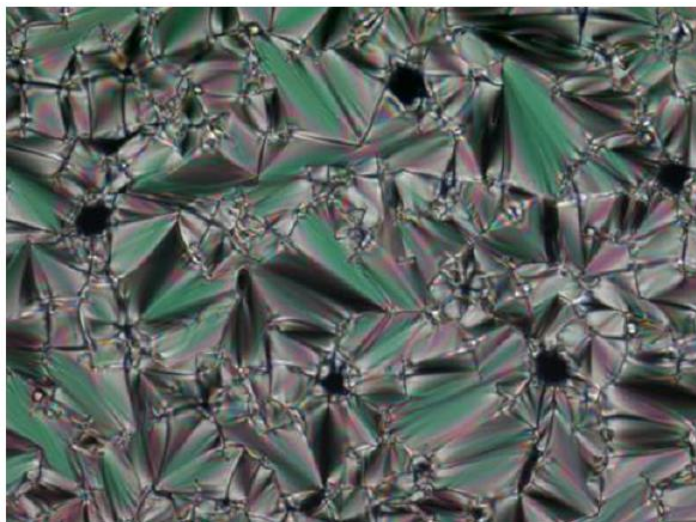


**Figure 2.28** SmA mesophase of 2-Alkoxy-5-phenylpyrimidines ( $n = 5$ ), displaying a fan-shaped texture under crossed polarizers upon cooling from the isotropic liquid [46].

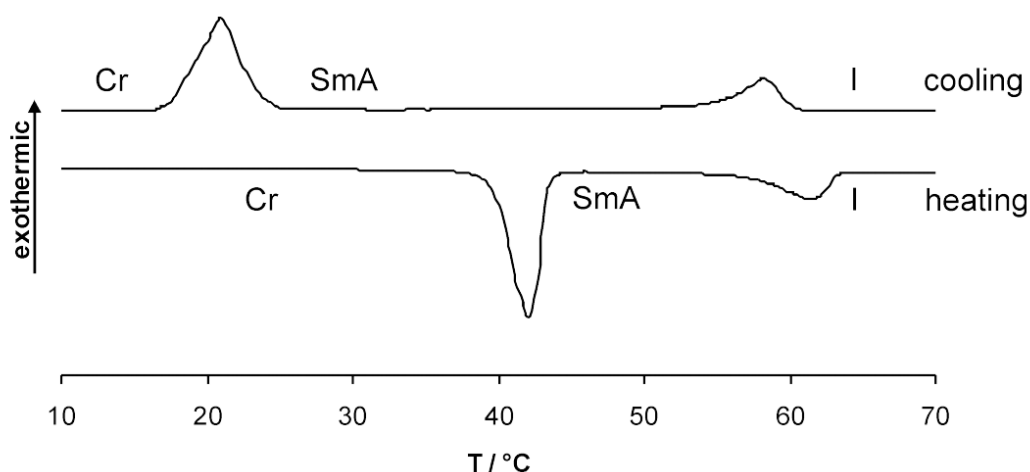


**Figure 2.29** DSC curve of 2-Alkoxy-5-phenylpyrimidines ( $n = 6$ ) [46].

In addition, Wang *et al.* had described that the spacer chain length (the number of carbon atom in the spacer of the mesogen) could be the driving factor to determine which type of a mesophase a compound will adopt [47]. In his work, he had synthesized symmetrical liquid crystal dimers containing hydrazide group with terminal hexadecyloxy chain (**Figure 2.30**).

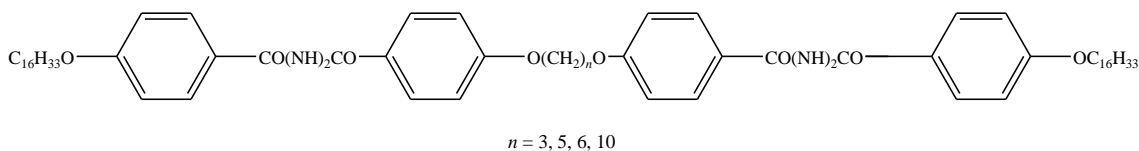
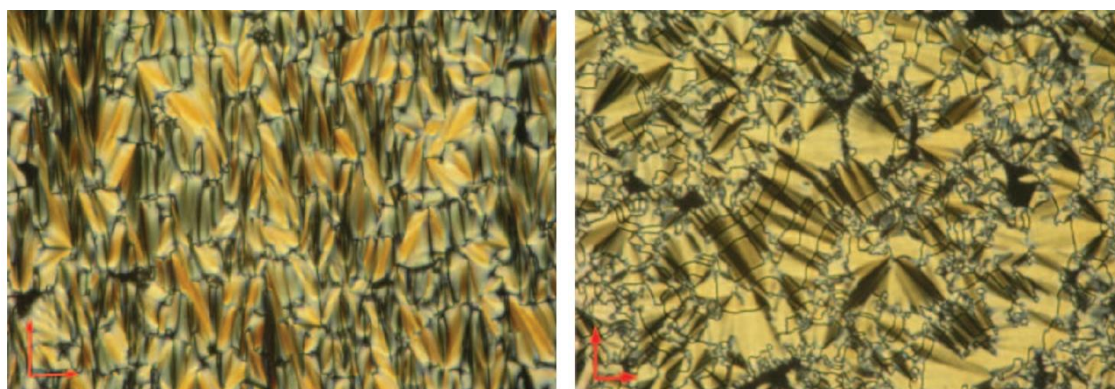


**Figure 2.30** Mesogenic dimer bearing hydrazide group [47].

Interestingly, those compounds with an odd number of carbon atoms in the spacer exhibited a smectic A mesophase, whereas compounds with an even number of carbon atoms in the spacer exhibited smectic C mesophase (**Figure 2.31**).



(a)

(b)

**Figure 2.31** A distinct difference between: (a) SmA (focal conic texture); and (b) SmC (fan-shaped texture). The red arrows indicate the direction of the polarisers [47].

Discotic liquid crystals commonly exhibit two types of mesophase, namely nematic discotic [48] and columnar hexagonal [49], abbreviated as  $N_D$  and  $Col_h$  respectively (**Figure 2.32**).

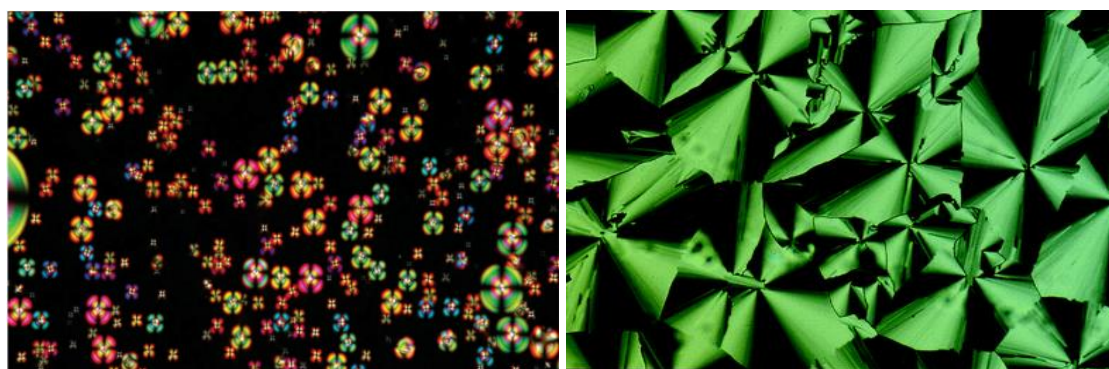


**Figure 2.32** An optical texture of (a)  $N_D$  [48]; and (b)  $Col_h$  [49].

## 2.8. Theoretical concepts

The ultimate goal of theoretical chemistry is to provide an *ab initio*, quantitative description of molecules and their reaction. To achieve this, knowledge of the exact structure and bonding in a molecule as well as detailed insight into the state-to-state dynamics which determine the outcome of a reaction are required. These insights are essential to understand the results from the increasingly sophisticated experiments.

Comparison with experiments also allows fundamental theories about structure, bonding and reactions to be tested. In recent years, accurate calculations on molecules, their spectroscopic data and state-resolved chemical process have become feasible owing to the tremendous progress in computational power. Moreover, the computational methods have developed to the point where they have sufficient accuracy to estimate reliable predictions for molecules that have not yet been made or reactions that have not yet been measured in the laboratory. An example of FTIR spectra comparison is given in **Figure 2.33** [50].

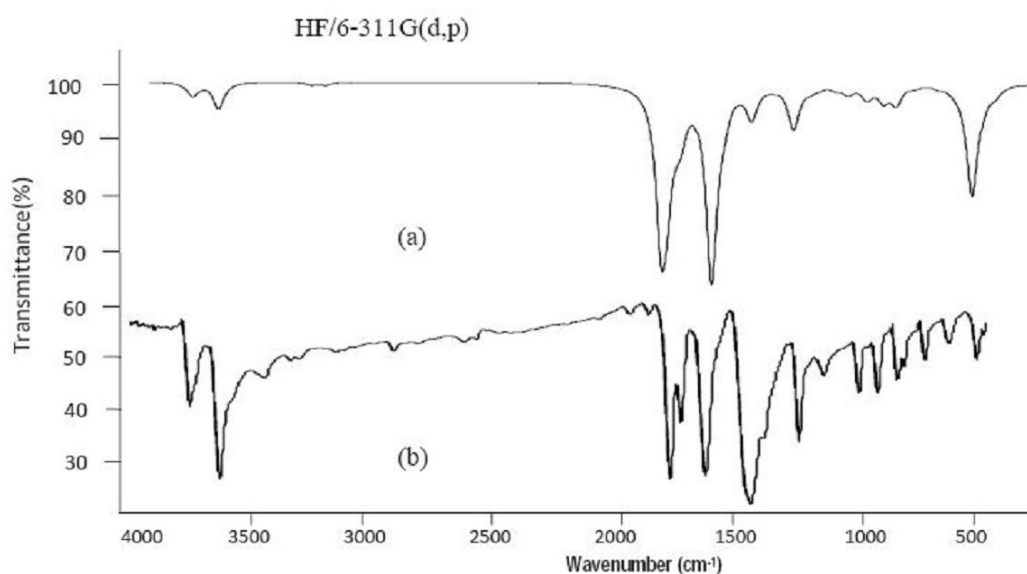


**Figure 2.33** FTIR spectra of 2-chloro-4-nitroaniline: (a) calculated and (b) observed [50].

Theoretical simulation is also a useful tool in predicting the optimized structure of a particular complex quantitatively. The study could also be extended to determine the nucleophilic and electrophilic sites obtained from the molecular electrostatic potential surface map (**Figure 2.34**) [51].

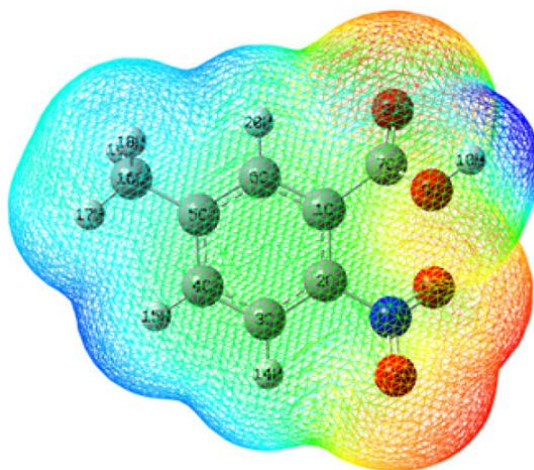


**Figure 2.34** Molecular electrostatic potential surface of 6-nitro-*m*-toluic acid [51].

The studies are also extended to the frontier molecular orbital analysis (the highest occupied molecular orbital (HOMO) and the lowest unoccupied molecular orbital (LUMO)) to predict the band gap energy and the occurrence of charge transfer within a molecule.

Atoms occupied by higher densities of HOMO will be more ready to detach an electron. In reciprocal, LUMO represents the ability to accept electrons, and atoms with a higher LUMO occupancy will easily gain an electron. On that account, HOMO and LUMO orbital energy could also be expressed as ionization energy,  $I$  ( $I = -E_{\text{HOMO}}$ ) and electron affinity,  $A$  ( $A = -E_{\text{LUMO}}$ ) respectively [51]. Analysis of HOMO – LUMO could be applied to calculate the molecular hardness, chemical potential and global electrophilicity in a molecule.

Molecular hardness,  $\eta$  is an important parameter to measure the resistance of a molecule towards electronic changes, which reflects the chemical stability of the molecule. The hardness of a molecule increases with the larger separation of energy ( $\eta = \frac{1}{2} (-E_{\text{HOMO}} + E_{\text{LUMO}})$ ) [52]. Hence, molecules with larger energy gaps are relatively considered as hard and molecules with smaller energy gap are considered as soft. Soft molecules are more polarizable since they only need smaller amount of energy to excite electrons from HOMO to LUMO.

## References

- [1] Housecroft, C.E., Sharpe, A.G. *Inorganic Chemistry* (2<sup>nd</sup> ed), (2005) Essex, England: Pearson Education Limited.
- [2] Singh, B.K., Bhojak, N., Mishra, P., Garg, B. S. *Spectrochim. Acta* (2008) A70, 758-765.
- [3] Patitungkho, S., Adsule, S., Dandawate, P., Padhye, S., Ahmad, A., Sarkar, F. H. *Bioorg. Med. Chem. Lett.* (2011) 21, 1802-1806.
- [4] Laidler, D.A., Milner, D.J. *J. Organomet. Chem.* (1984) 270, 121-129.
- [5] Valko, M., Mazur, M., Morris, H., Klement, R., Williams, C. J., Melnik, M. J. *Coord. Chem.* (2000) 52, 129-138.
- [6] Joy, R.A., Arman, H., Xiang, S., Musie, G. T. *Inorg. Chim. Acta* (2013) 394, 220-228.
- [7] Jiang, X., Xia, H., Zhu, Y. -F., Huang, C. -X., Liao, Y. -H., Z. *Anorg. Allg. Chem.*, (2011) 637, 2273-3277.
- [8] Wannarit, N., Siriwong, K., Chaichit, N., Youngme, S., Costa, R., Moreira, I. P. R., Illas, F. *Inorg. Chem.* (2011) 50, 10648-10659.
- [9] Hamza, F., Kickelbick, G. *Macromolecules* (2009) 42, 7762-7771.
- [10] Moncol, J., Vaskova, Z., Stachova, P., Svorec, J., Silanpaa, R., Mazur, M., Valigura, D. *J. Chem. Crystallogr.* (2010) 40, 179-184.
- [11] Yu, Y. -H., Ren, C. -Y., Hou, G. -F., Ye, H., Gao, J. -S. *J. Coord. Chem.* (2012) 65, 4137-4146.
- [12] Pajtasova, M., Ondrusova, D., Jona, E., Mojumdar, S. C., L'Alikova, S., Bazylakova, T., Gregor, M. *J. Therm. Anal. Calorim.* (2010) 100, 769-777.
- [13] Agterberg, F.P.W., Provokluit, H. A. J., Driessen, W. L., Reedjik, J. Oevering, H., Buijs, W., Veldman, N., Lakin, M. T., Spek, A. L. *Inorg. Chim. Acta* (1998) 267, 183-192.
- [14] Iqbal, M., Ahmad, I., Ali, S., Muhammad, N., Ahmed, S., Sohail, M. *Polyhedron* (2013) 50, 524-531.
- [15] Mosae, S.P., Nadella, S., Sahoo, Jashobanta., Suresh, E., Subramaniam, P.S. *J. Coord. Chem.*, doi 10.1080/00958972.2012.755521
- [16] Wein, A.N., Cordeiro, R., Owens, N., Olivier, H., Hardcastle, K. I., Eichler, J. F. *J. Fluorine Chem.* (2009) 130, 197-203.
- [17] Bird, M. J., Lomer, T. R. *Acta Crystallogr. Sect. B:* (1972) 28, 242-246.
- [18] Lomer, T. R., Perera, K. *Acta Crystallogr. Sect. B:* (1974) 30, 2912-2913.

- [19] Lomer, T. R., Perera, K. *Acta Crystallogr. Sect. B*: (1974) 30, 2913-2915.
- [20] Ramos, R.M., Martinez, C. F. J., Lopez-Andres, S., Garcia, P. M. V., Redondo, Y. M. I., Torres, M. R., Garrido, L., Rodriguez, C. J. A. *Cryst. Growth Des.* (2008) 8, 2547-2554.
- [21] Petrič, M., Leban, I., Šegedin, P. *Polyhedron* (1995) 14, 983-989.
- [22] Petrič, M., Leban, I., Šegedin, P. *Polyhedron* (1996) 15, 4277-4282.
- [23] Lindoy, L.F. *The Chemistry of Macrocyclic Ligand Complexes.* (1989). Melbourne, Australia: Press Syndicate of the University of Cambridge.
- [24] Bosnich, B., Poon, C. K., Tobe, M.L. *Inorg. Chem.* (1965) 4, 1102-1108.
- [25] Bandoli, G., Dolmella, A., Gatto, S. *J. Crystallogr. Spectrosc. Res.* (1993) 23, 755-758.
- [26] Meyer, M., Dahaoui-Gindrey, V., Lecomte, C., Guillard, R. *Coord. Chem. Rev.* (1998) 178–180, 1313-1405.
- [27] Kim, J. C., Lough, A.J., Park, H., Kang, Y.C. *Inorg. Chem. Commun.* (2006). 9, 514-517.
- [28] Lim, S. L., Ng, C. H., Teoh, S. G., Loh, W. –S., Fun, H. –K. *Acta Crystallogr. Sect. E*: (2010) 66, m737-m738.
- [29] Lindoy, L. F., Mahinay, M. S., Skelton, B., White, A. H. *J. Coord. Chem.* (2003) 56(14), 1203-1213.
- [30] Ahmad Tajidi, N.S., Abdullah, N., Arifin, Z., Tan, K. W., Ng, S. W. *Acta Crystallogr. Sect. E*: (2010) 66, m889.
- [31] Zeleňák, V., Vargová, Z., & Györyová, K. *Spectrochim. Acta Part A*: (2007) 66, 262-272.
- [32] Redondo, M. I., Garcia, M. V., Gonzalez-Tejera, M. J., Cheda, J. A. R. *Spectrochim. Acta Part A*: (1995) 51, 341-347.
- [33] Moreno, V., Dittmer, K., Quagliano, J. V. *Spectrochim. Acta* (1960) 16, 1368-1381.
- [34] Baran, E. J., Viera, I., Torre, M. H. *Spectrochim. Acta Part A*: (2007) 66, 114-117.
- [35] Cabaniss, S. E., McVey, I. F. *Spectrochim. Acta Part A*: (1995) 51, 2385-2395.
- [36] Martini, D., Pelli, M., Pettinari, C., Skelton, B. W. *Inorg. Chim. Acta* (2002) 333, 72-82.
- [37] Deacon, G. B., Phillips, R. J. *Coord. Chem. Rev.* (1980) 33, 227-250.
- [38] Gómez-Saiz, P., Garcia-Tojal, J., Maestro, M. A. Mahia, J. Arnaiz, F. J., Rojo, T. *Polyhedron* (2002) 21, 2257-2263.

- [39] Vafazadeh, R., Hayeri, V., Willis, A. C. *Polyhedron* (2010) 29, 1810-1814.
- [40] Maldonado-Rogado, M. A., Vinuelas-Zahinos, E., Luna-Giles, F., Bernalte-Garcia, A. *Polyhedron* (2007) 26, 1173-1181.
- [41] García-Tojal, J., Lezama, L., Pizarro, J. L., Insausti, M., Arriortua, M. I., Rojo, T. *Polyhedron* (1999) 18, 3703-3711.
- [42] Meiklejohn, R. A., Meyer, R. J., Aronovic, S. M., Schuette, H. A., Meloche, V. W. *Anal. Chem.* (1957) 29, 1112-1112.
- [43] Burrows, H. D., Ellis, H. A. *Thermochim. Acta* (1982) 52, 121-129.
- [44] Muhammad, K., Hameed, S., Tan, J., Liu, R. *Liq. Cryst.* (2011) 38, 333-348.
- [45] Santos-Martell, R. G., Ceniceros-Olguin, A., Larios-Lopez, L., Rodriguez-Gonzalez, R. J., Navarro-Rodriguez, D., Donnio, B., Guillon, D. *Liq. Cryst.* (2009) 36, 787-797.
- [46] Starkulla, G. F., Kapatsina, E., Baro, A., Giesselmann, F., Tussetschlager, S., Kaller, M., Laschat, S. *Beilstein J. Org. Chem.* (2009) 5, pages not available.
- [47] Wang, H., Bai, B., Gong, C., Zhang, P., Li, F., Li, M., Clark, N. A. *Liq. Cryst.* (2008) 35, 967-974.
- [48] Gardner, D.F., Julian, S. E., Smalyukh, I. I. *Mol. Cryst. Liq. Cryst.* (2011) 545, 1227-1245.
- [49] Yokoyama, H. *Nat. Photon* (2009) 3, 560-561.
- [50] Udhayakala, P., Jayanthi, A., Rajendiran, T. V., Gunasekaran, S. *Int. J. ChemTech Res.* (2011) 3, 1851-1862.
- [51] Balachandran, V., Karthick, T., Perumal, S., Nataraj, A. *Spectrochim. Acta Part A:* (2012) 92, 137-147.
- [52] Eckhardt, C. J. *Mol. Cryst. Liq. Cryst.* (2006) 456, 1-14.